

Stride Period Adaptation for a Biomimetic Running Hexapod

Jorge G. Cham, Jonathan Karpick, Jonathan E. Clark, Mark R. Cutkosky

Stanford University Center for Design Research
Stanford, CA 94305, jgcham@cdr.stanford.edu

Abstract

We demonstrate an adaptation strategy for adjusting the stride period in a hexapedal running robot. The robot is inspired by discoveries about the self-stabilizing properties of insects and uses a sprawled posture, a bouncing alternating-tripod gait, and passive compliance and damping in the limbs to achieve fast, stable locomotion. The robot is controlled by an open-loop clock cycle that activates the legs at fixed intervals. For maximum speed and efficiency, this imposed stride period should be adjusted to match changes in terrain (e.g. slopes) or loading conditions (e.g. carrying an object). An ideal adaptation strategy will complement the design philosophy behind the robot and take advantage of the self-stabilizing role of the mechanical system. In this paper we describe an adaptation scheme based on measurements of ground contact timing obtained from binary sensors on the robot's feet. We discuss the motivation for the approach, putting it in the context of previous research on the dynamic properties of running machines and bouncing multi-legged animals, and show results of experiments.

1. Introduction

We have built a family of hexapedal robots that are inspired by discoveries concerning the locomotion of insects and, in particular, of the cockroach. These animals run rapidly (between 10 and 50 body-lengths/second depending on the species) over rough terrain using a combination of open-loop muscle activation patterns and "preflexes," i.e., passive mechanisms that stabilize the animals' motion in response to perturbations [1][2][3][4]. Like the insects that inspired them, the robots employ passive mechanical properties that enable them to run quickly (over 3 body-lengths per second) and over hip-height obstacles (see Fig. 1) without complex closed-loop control [5]. Although this approach works well in the laboratory, there is a question about its versatility. How effectively can a particular open-loop control and set of mechanical properties function over a range of conditions which may include variations in ground slope and hardness and changes in loading? Furthermore, the animals or robots themselves may change over time. A limb may become damaged or the mechanical properties may vary with temperature. A way to address this problem is adaptation, in which the parameters of the open-loop control are automatically adjusted to optimize performance as conditions change.

Figure 2 illustrates an approach in which adaptation is combined with reflexes for stable running. An open-loop, feed-forward, motor controller generates the pattern of actu-

ator commands to achieve a steady alternating-tripod gait. The kinematic arrangement and passive compliance and damping of the limbs achieve the locomotion and provide stable response to perturbations. In running insects, an important reason for employing slow adaptation in combination with reflexes is that neural conduction speeds are too slow for feedback control to act during each stride period. In robots, of course, the same limitation does not necessarily apply. However, for small and inexpensive robots like *Sprawlita*, the same approach allows the use of simple sensors without concerns that actuator delays, sensor noise or even failures will jeopardize short-term performance. This is an important consideration because many sensors become noisy when mounted on a small hexapod running at 7-10 Hz.

The basic design of the *Sprawl* family of hexapods consists of a body and legs built up in layers using a rapid-prototyping process called Shape Deposition Manufacturing. The design and manufacturing details have been presented elsewhere [5][6]. Each leg has two degrees of freedom but only the thrust direction is actuated, using pneumatic pistons embedded into the legs. When running, hip rotations are passive and are accomplished by flexures of visco-elastic material. This design is inspired by the mostly passive tro-

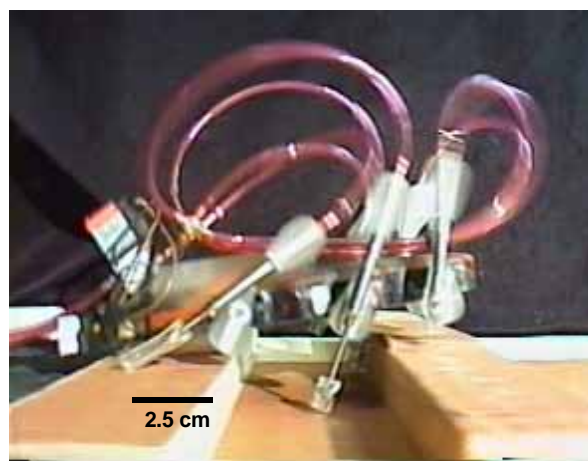


Figure 1. The hexapedal robot has a body and legs fabricated by Shape Deposition Manufacturing [5] and features embedded actuators and compliant legs. Here the robot is crossing a belly-height obstacle without using sensory feedback and without significantly slowing down or being knocked off course.

chanter-femur joint in cockroaches. A servomotor at each hip is used only to establish the equilibrium position of the hip joint. Binary contact sensors are attached to the feet. The original Sprawlita design uses two pneumatic valves, one for each tripod, embedded into the body of the robot. A newer design has a valve embedded into each leg. This arrangement results in faster actuator dynamics and more control over the timing of the thrust force at each foot. As will be seen in the following sections, these are important considerations. Depending on configuration, the robots weigh between 0.25-0.33 Kg and have a length of 10-15cm. Maximum speeds range from 0.5-0.8m/sec with preferred stride frequencies of 7-10 Hz.

The locomotion parameters that can be varied are the stride period (length of time between activation of each tripod), the duty cycle (length of time that the valves are kept open during each stride) and the equilibrium positions of the compliant hip joints. All of these parameters contribute to running performance and could be subject to adaptation. In this paper, we focus on stride period and duty cycle.

Figure 3 illustrates the value of adjusting the stride frequency. At low frequencies, the speed of the robot increases more or less linearly with stride frequency. However, at frequencies above 10 Hz, we become limited by actuator dynamics and the speed actually drops because the pistons are not able to produce their maximum thrust. On level ground the fastest locomotion is obtained with a frequency of approximately 10 Hz. But on a 20 degree slope, locomotion is considerably faster at 5 Hz than at 10 Hz. The optimal frequency also varies somewhat from one robot to the next

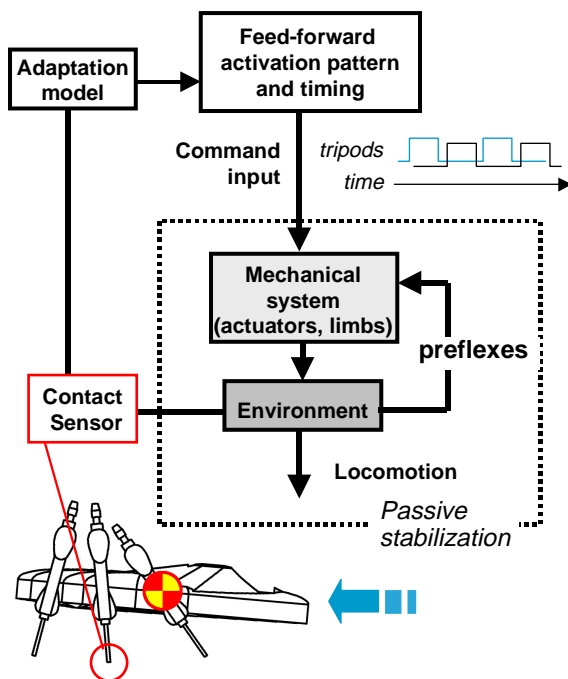


Figure 2. A combination of stabilizing passive mechanisms, or "preflexes," and sensor-based adaptation of an open-loop feed-forward controller provides insects and small robots with a robust, stable and versatile approach to running over rough terrain.

due to manufacturing tolerances and variations in the materials properties of the legs. Consequently, there is a motivation to make the robots "self-tuning" over a range of operating conditions. Ideally, we would like an adaptation strategy that does not require adding expensive or complicated sensors to the robot.

For these reasons, we were lead to examine the relationship between ground contact times (obtained from binary sensors in the robots' feet) and the timing parameters (frequency and duty cycle) of the open-loop motor control. As will be discussed in Section 3, of the various timing quantities that we can examine, the interval between end of thrust (closing of the pneumatic valve) and liftoff of the feet provides the best indication for adjusting the stride frequency. To understand better why this approach works, we first examine a simplified one-legged vertical hopper model.

2. Simplified Model for Open-Loop Locomotion and Adaptation

To understand how monitoring the ground contact time can provide information about the effectiveness of running, we start with a simple hopping model that has been examined extensively in the literature. Although this model cannot tell us about the coupling between vertical and horizontal motion, an important factor in the dynamics of the Sprawl robot family, it does shed light on the relationship between hopping height and actuator timing. It helps us to understand under what circumstances a stable, steady-state hopping height is achieved with an open-loop control scheme and to determine how to get the most work out of our actuators with the simplest of sensors.

Variations on this basic model have been examined by Raibert [7], Koditschek and Buehler [8], Ringrose [9], and Berkemeier and Desai [10]. Despite its apparent simplicity, the one-legged vertical hopper exhibits a rich set of dynamic behaviors including stable and unstable periodic motion.

Raibert's hopper [7] uses a double-acting pneumatic cylinder and an actuated hip to produce forward motion. The cylinder acts as an air spring when its valves are closed, providing a system similar to the simplified hopper of Fig-

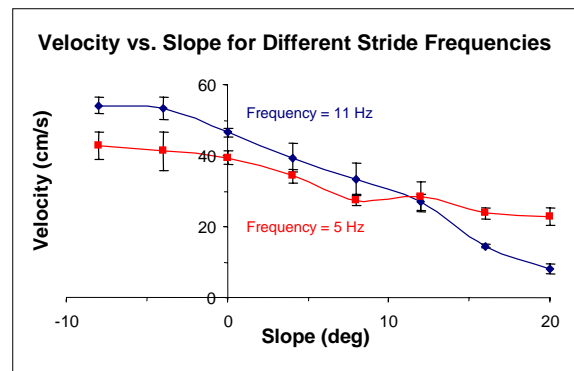


Figure 3. Ground speed versus stride period on level ground versus slope. As shown, the optimal stride period for maximum speed depends on the slope, which illustrates the need for adaptation.

ure 4, although with a $1/r$ spring. Thrust is applied in a closed-loop fashion when the leg is sensed to be at maximum compression. Height is varied by changing the thrust duration. The stability of a simplified one-DOF hopper model based on this closed-loop thrust activation is analyzed by Koditschek and Buehler [8].

Ringrose [9] designed a vertical hopper that maintains stable hopping without sensory feedback, using a linear actuator in series with a spring, and a damper in parallel with the actuator/spring combination. For analysis, Ringrose uses a simplified model in which thrust is applied through an impulsive change in leg length, which occurs before maximum compression of the spring.

Berkemeier and Desai [10] compare Raibert's method of applying thrust at maximum compression, Ringrose's open loop control, and a proposed "adaptive periodic forcing" method that adjusts the period of the open loop control based on the velocity at the time that thrust is applied. In their analysis, they use a hopper with a spring and damper in parallel and an actuator that changes the neutral point of the spring. Their analysis shows that their hopper reaches maximum hopping height when the force is applied at maximum spring compression. They also show that, for low values of damping, the motion is stable, without feedback, when the force is applied prior to the maximum compression of the spring and unstable when the force is applied after the maximum compression.

Komsuoglu and Koditschek [11] analyze the stability of a similar open-loop one-DOF hopper in which thrust is effected by clock-driven changes in stiffness and find conditions for stability, which include the necessary presence of viscous friction.

The physical implementation of the Sprawl robots requires that the minimal damping assumptions made in previous models be reviewed. In insects, and in the Sprawl family of robots, viscoelastic materials dissipate substantial amounts of energy per cycle. Typical dimensionless damping ratios are on the order of $\zeta = 0.3$ [12]. Additionally, a model was needed to determine the practicality of using a

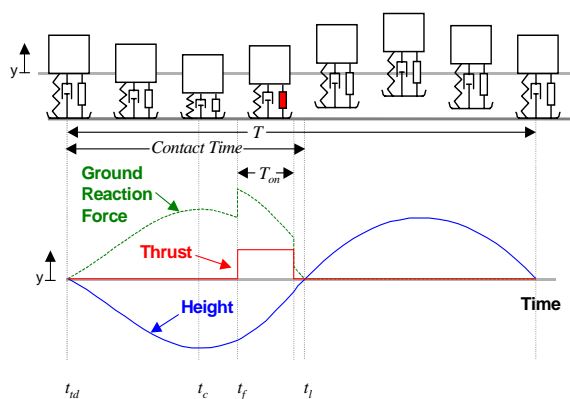


Figure 4. Time history of a single degree-of-freedom vertical hopper. The mass is attached to a massless leg with stiffness k and damping b . At some time t_f a thruster in parallel applies a force, F . At some time t_l , the mass lifts off the ground and travels ballistically in the air.

simple binary switch for feedback instead of more complicated and noise-susceptible velocity sensors.

We therefore consider a single-legged vertical hopper which can include substantial viscous damping. Figure 4 depicts a sample time history of this hopping model. The massless leg has stiffness, k , damping, b , and an actuator that is able to provide a thrust force $f(t)$ that is initiated at some time t_f and terminated after a fixed duration, T_{on} , or by liftoff, whichever occurs first. The stride period begins at $t=0$ as the robot touches down, which occurs when $y=0$, the spring's neutral length. During the ground contact phase, the ground reaction force is given by:

$$GRF = ky + b\dot{y} - f(t)$$

where k is the spring constant, b is the viscous damping constant and $f(t)$ is the actuator force. The equation of motion for the mass is therefore

$$m\ddot{y} = -ky - b\dot{y} - g + f(t)$$

Liftoff occurs when the ground reaction force is equal to zero, and the hopper transitions to an airborne phase, where it travels ballistically. In the next two sections, we consider the conditions for optimal hopping height of this model, and conditions for the existence of stable behavior.

2.1 Optimal hopping height

In steady-state, the landing velocity of one cycle must equal the landing velocity of the previous cycle. Simulations were conducted to determine which values of force application

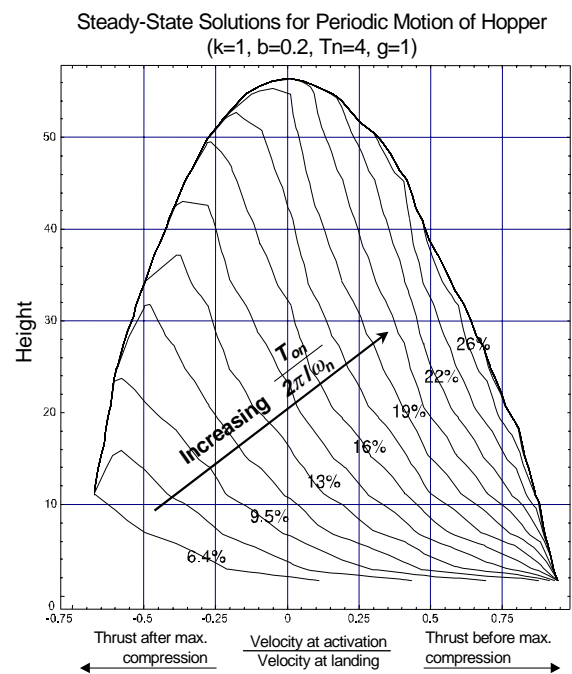


Figure 5. Hopping height as a function of normalized velocity at Thrust application for the one-DOF hopper. Each line represents the solutions to the steady-state constraint equations for a given set of operating parameters and as the thrust duration is varied.

time, t_f , and force duration, T_{on} , meet steady state conditions for given values of m, k, b, g , and force T_n . For example, the steady state hopping height versus the velocity at which thrust is initiated for $m=g=k=1, b=0.2$, and $T_n=4$ are shown in Figure 5 for a range of thrust durations.

Figure 5 shows that for thrust duration times greater than 20% of the natural period, peak hopping height is achieved when the thrust is applied near the point of maximum spring compression, that is, when the velocity at activation is nearly zero. For shorter thrust durations, however, optimal steady-state hopping heights occur when thrust is initiated *after* maximum spring compression (velocity at force application is positive).

In evaluating the conditions that determined the maximum hopping heights in Figure 5, it was found without much surprise that for a given force level and duration, the maximum hopping height is obtained by maximizing the work added to the system by the actuator:

$$\int_{t_f}^{(t_f + T_{on})} f(t) \cdot \dot{y}(t) dt = WorkInput$$

If $f(t)$ is constant, it is clear that for a long thrust that is applied until the end of the ground contact phase, this integral is maximized when thrust activation, t_f , coincides with maximum compression. For a short thrust duration which ends before the end of the ground contact phase, the conditions for the maximization of this integral are more complex, but can be shown to roughly coincide with maximizing the upward velocity at thrust activation (while still achieving end-of-thrust before lift-off).

2.2 Stability and multiple solutions

The plot in Figure 5 shows an example set of solutions to the steady-state constraint equations. With open-loop control, the system will either converge to one of the steady-state solutions from Figure 5, converge to more complicated hopping patterns, or assume non-periodic behavior. In practice, as we varied the open-loop timing parameters, we found that the simulations converge to different steady-state behaviors, and often don't converge to periodic motion at all. To study the effects of changing the timing parameters on behavior and stability, we considered the local stability of the steady-state solutions.

The steady-state motion of the hopper model is determined by its return map:

$$X_{n+1} = F(X_n)$$

which relates the state after one cycle, X_{n+1} , to the previous state, X_n , for a given set of operating conditions [13]. Steady-state solutions satisfy:

$$X^* = F(X^*)$$

and are called "fixed points." Although the equations of motion that govern the ground-contact and airborne phases are linear, the transitions between the two phases make the return map non-linear and, in this case, intractable to solve

explicitly. The local stability of each existing solution is given by the linearized return map, a Jacobian matrix, M , defined as:

$$\delta X_{n+1} = M(X_n) \delta X_n$$

where,

$$M(X_n) = \frac{\partial}{\partial X_n} F(X_n)$$

If the eigenvalues of the matrix M evaluated at the fixed point are within the unit circle, then the fixed point is locally stable, since $M(X^*)$ maps disturbances about the fixed point from one cycle to the next [13]:

$$|eig(M(X^*))| < 1$$

The return map and the matrix M were found analytically for our one-DOF model using only the simplifying assumption that lift-off occurs when $y=0$. The two cases considered in this analysis were: a) when thrust application ends at or after lift-off (termed "Long Thrust"); and b) when thrust application ends before lift-off (termed "Short Thrust"). The analytical equations used in the following results are found in the Appendix.

Figure 6 shows a typical example of the effects of changing the open-loop stride period for the "Long Thrust" case, for a given thrust magnitude, T_n , natural frequency, ω_n , and damping ratio, z . For short periods, hopping height starts out very small, and thrust application starts well before maximum compression (given by the negative normalized velocity at application). These solutions are termed "Regular Hopping" as they represent a desired mode of hopping behavior. As the period is increased, hopping height increases, and velocity at application approaches zero. Finally, at a certain period (near 275ms period), height is maximized when velocity at application is nearly zero, as predicted. However, as the period approaches 275ms the magnitude of the eigenvalues quickly increases and the solution becomes unstable. Simulations of the hopper, though, never reach this point. As shown in the figure, a second set of solutions appears at a period near 250ms. These solutions are termed "Hop-settle-fire" as the mass has started to settle before thrust is applied. The hopping height for this solution is much lower, but its corresponding eigenvalues are also much lower, and the simulations converge to this solution.

Figure 7 shows a typical example of the effects of changing the open-loop stride period for the "Short Thrust" case. For short periods, the solutions start out as "Regular Hopping." However, as period is increased, the eigenvalues start to move outside the unit circle. Simulations for this range are "period-1 unstable" (the state does not repeat after one cycle), but tend to be "period-2 stable" (the state repeats after two cycles). As the period is further increased, the "Regular Hopping" solutions become stable again. The velocity at thrust activation also increases, and changes from negative (thrusting before maximum compression) to positive (thrusting after maximum compression). Maximum

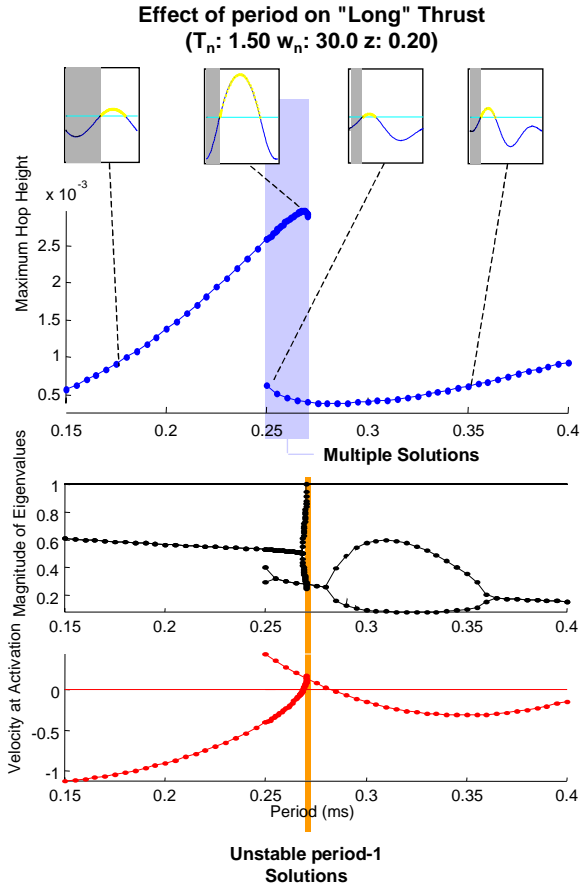


Figure 6. Effects of changing the stride period on steady-state motion and stability for the one-DOF hopper case in which thrust application ends at or after lift-off.

hopping height is also increased with period and keeps increasing until the solutions end. However, near 275ms period another chain of valid steady-state solutions begins. This is the “Hop-settle-fire” solution for the “Long Thrust” case, in which hopping height is lower. Simulations converged to this solution presumably because of its lower eigenvalues. Finally, as period is further increased, simulations converge to “Hop-settle-fire” solutions for the “Short Thrust” case, as thrust application ends before lift-off.

A rigorous analysis of the effects of the model’s other parameters on the hopping motion is beyond the scope of this paper, but they are nonetheless stipulated here from experience with the simulations. The onset of the “Hop-settle-fire” solutions is determined largely by the system’s natural frequency. These solutions become available when the period of thrust application is long enough that the system is allowed to settle according to its natural period. The addition of damping also makes these solutions possible, since without damping the system would not settle. Decreasing damping and increasing the thrust magnitude and duration all seem to have a destabilizing effect, as they extend the region of unstable solutions.

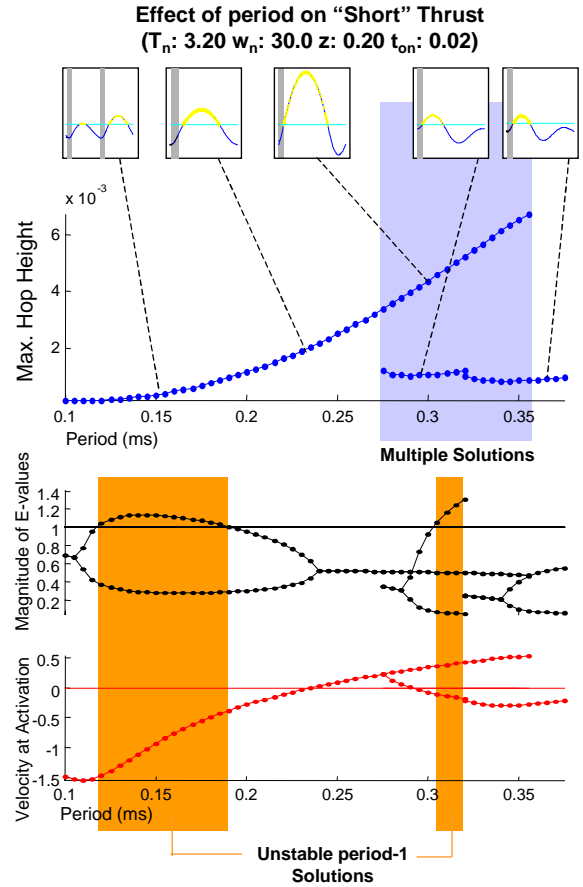


Figure 7. Effects of changing the stride period on steady-state motion and stability for the one-DOF hopper case in which thrust application ends before lift-off.

2.3 One-DOF model conclusions

As shown above, maximum height is achieved when the open-loop stride period is such that the positive work done by the thrust application is maximized. In general, for both the “Long Thrust” and “Short Thrust” cases, this occurs when the open-loop stride period results in a stable solution in which thrust application starts “as late as possible” and ends shortly before or at lift-off, given by the leg reaching its end-of-stroke. An adaptation strategy to increase hopping height would set the thrust application period according to these two general guidelines. However, as will be shown in the following section, for a multi-degree-of-freedom system such as our robot, horizontal ground speed may depend on the stride period, or stride frequency, in other ways.

3. Stride Period Adaptation

3.1 Robot performance tests

The one-DOF model provided insight into the basic behavior of an open-loop hopping system with passive properties in terms of the work performed by the actuator and the resulting performance. In order to develop an adaptation law

for the six-legged, multi-DOF robot, we must look at the factors that affect its performance and see whether the same basic mechanisms are evident. Figure 8 shows the performance results of the hexapedal robot as a function of open-loop stride period on flat ground. As shown in 8a, increasing the stride period causes the vertical oscillations, $\Delta height$, to increase, similar to the one-DOF model. Figure 8b shows the difference between the time that a particular tripod is deactivated, T_d , and the time that the middle-foot of that tripod leaves the ground, T_a . This time lag, $(T_d - T_a)$, is increasingly positive for longer periods, which indicates that thrust application ends after lift-off, here caused by end-of-stroke. This quantity also monotonically increases for longer periods since thrust application, or T_{on} , is set as a fixed percentage, or duty cycle, of the stride period. However, note that the time lag is a nearly constant small value for periods around 130ms, where the robot is running fastest.

The trade-off between vertical oscillations and ground speed is that, while increased vertical oscillation may entail longer strides, the stride frequency (strides per second) is a dominant factor in determining ground speed. However, decreasing the stride period eventually runs into the limitations of the thrust mechanisms described by the one-DOF model and into the limitations of the actuators. As shown in Figure 8b, the time lag, $(T_d - T_a)$, approaches zero as the period decreases, indicating that thrust application is being terminated closer to the time that end-of-stroke occurs. Below the optimal period the time lag remains nearly constant since ground contact is lost due to leg retraction when the valves are deactivated. This behavior, combined with the fact that the bandwidth of the pneumatic actuator system starts to be exceeded at the low stride periods, results in the ineffective application of thrust, as evidenced by the sharp drop in ground speed.

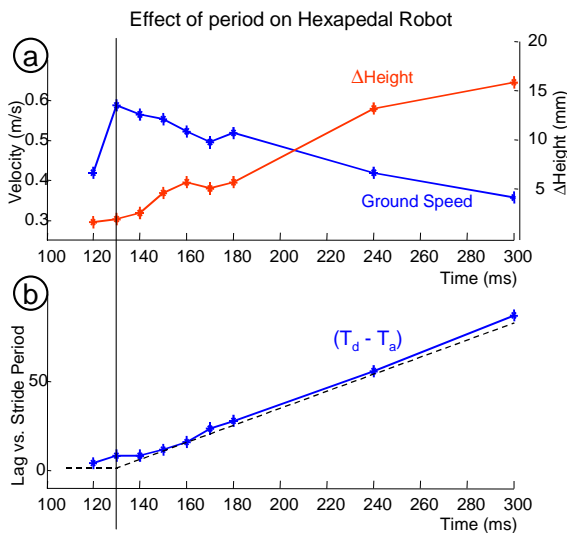


Figure 8. Performance tests for the hexapedal robot in flat ground as a function of open-loop stride period with constant duty cycle percentages.

The change in slope of the time lag, $(T_d - T_a)$, just above the period of optimal ground speed is used as the basis for the simple adaptation law described in the following section.

3.2 Adaptation strategy

The results from the previous sections motivate the robot stride period adaptation strategy described here. As illustrated by the one-DOF model, it is advantageous to end thrust “late” in order to maximize work input. However, due to the limitations of the pneumatic system, thrust duration and frequency must be limited in order to obtain full stroke in extension and retraction.

A prototype adaptation law for maximizing ground speed that takes these findings into consideration using foot contact information is as follows:

$$\tau_{n+1} = \tau_n + K_i - K_p(T_d + T_v - T_a)$$

Here, K_i and K_p are adaptation gains, T_v is a constant offset parameter and T_d and T_a are the measured valve deactivation and lift off times. Figure 9 illustrates what these quantities represent, where time is measured with respect to the initiation of the gait cycle, which starts when the valve for one of the tripods is activated. The adaptation law is based on a binary switch attached to the middle foot of the same tripod. T_d is determined by the stride period, τ_n , and duty cycle, T_{on} , which in this case is specified as a fixed percentage of the stride period. If there is no measured ground contact information, T_a , then the period is not modified.

Intuitively, this simple adaptation law can be described as trying to decrease the stride period as much as possible without exceeding the bandwidth of the actuators and without terminating the thrust application before end-of-stroke (to maximize available work). Here, K_i is a “drift” term which is trying to increase the stride period at every step,

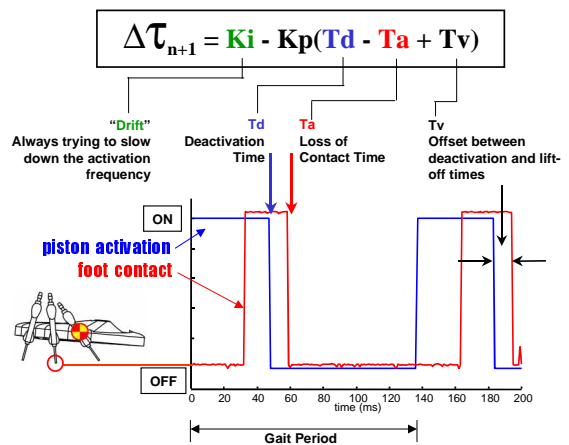


Figure 9. Simple gait period adaptation law based measured duration between foot contact events. A binary switch in the robot’s middle foot provides contact information. This time duration is compared to the actuator valve deactivation time for the adaptation law

since the difference between T_d and T_a is nearly constant for lower periods. The stride period reaches an equilibrium value when $\Delta\tau$ is zero, which occurs when $(T_d - T_a)$ reaches a nominal value. In this case, T_v is adjusted so that the equilibrium stride period maximizes ground speed.

3.3 Adaptation Results and Discussion

Figure 10 shows test results of the adaptation law implemented in the hexapedal robot running on flat ground. Each data point in Figure 10a represents the new stride period after one stride cycle, or learning loop, in which T_a (shown in Fig. 10b) was measured. The parameter T_v was chosen such that the equilibrium period coincided with the optimal period for flat ground found in Section 2. The gains K_i and K_p were experimentally chosen to give the adaptation a fast learning rate without causing instabilities. As shown in the figure, for starting periods that are lower than the equilibrium period, the learning rate is approximately linear, due to the predominance of the K_i term. For higher starting periods, however, the K_p term dominates and the learning rate is approximately exponential. Note from Figure 10b that, although only a simple contact switch was used, the measured values of T_a are still prone to some noise, due to ground imperfections or disturbances to the robot. Despite these variations, the adaptation of the stride period still proceeds smoothly, and does not affect the stabilization performed by the mechanical system throughout a particular stride.

For an uphill ground slope of 10 degrees, the adaptation strategy also converges to an equilibrium stride period. This new equilibrium period (165ms) is higher than the equilibrium period for flat ground running (130ms) and results in faster uphill running than with the optimal period for flat

ground. However, the new equilibrium period is still lower than the period found to be optimal at 10 deg. slope (190ms). This indicates that, although the adaptation strategy works to improve the locomotion, the factors that affect uphill running may need to be re-examined. For example, in seeking to increase the stride frequency for optimal ground speed in flat terrain, the prototype adaptation law presented here reduces vertical oscillations, which we postulate will have a significant role in climbing up-hill terrain.

4. Conclusions and Future Work

The analyses and experiments in the previous sections show that for an open-loop running robot, stride frequency and thrust duration are important parameters that govern hop height and forward speed. The single legged hopper model reveals that optimal hop height is obtained by maximizing the product of thrust force and velocity over the thrust duration. However, this product is subject to both dynamic constraints and hardware limitations. The dynamic constraints include the requirement of a stable, steady-state periodic solution to which the system will converge. Significant passive damping, as found in insects and in robots like Sprawlita, increases the regime of stable, periodic operation with open-loop forcing. The hardware limitations include the speed at which the piston can be filled and exhausted and the maximum thrust force available.

An adaptation strategy for the stride period that takes these limitations into account and tries to optimize ground speed was presented in this paper. The adaptation law seeks to maximize the stride frequency, and obtain the most work from the actuators without exceeding their bandwidth. This adaptation law uses only the sensed duration of ground contact during each stride, and was shown to cause the stride period to converge and to improve the speed even over changes in terrain and despite disturbances to the locomotion.

More generally, the adaptation scheme presented in this paper is an example of an approach that is particularly well suited for small, biomimetic robots. It requires no expensive or sophisticated sensing or feedback. Only binary sensors are needed to provide an estimate of ground contact time. The adaptation scheme takes advantage of the passive properties of the robot that allow it to run stably over a range of open-loop stride frequencies and actuator duty cycles. In the event of sensor failure, the performance of the robot degrades only to that of the open-loop system without adaptation. This approach allows the robots to remain simple, inexpensive and robust while also being able to "tune" themselves to accommodate individual variabilities and changes in operating conditions.

Future work will build upon the simple adaptation law tested in this paper to incorporate other simple sensor information (e.g. tilt sensor, contact switches in other feet) in order to increase performance and adaptability. As discussed previously, further understanding of the robot's dynamic interaction with different types of terrain such as sloped or compliant surfaces will allow us to increase the adaptation's versatility. Finally, future work will study the effects of

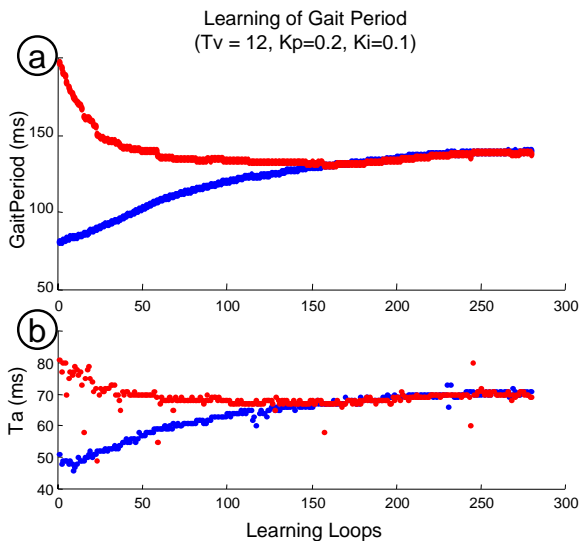


Figure 10. Adaptation results for gait period. (a) shows the adaptation of the gait period from two initial starting values. (b) shows the corresponding measured values of t_a for each gait period

such an adaptation law on other types of behavior, such as rapid turning and navigation.

5. Acknowledgments

We have been fortunate to collaborate with Professor Robert J. Full at the U.C. Berkeley Polypedal Laboratory throughout this work and to benefit from his prodigious knowledge and understanding of the mechanisms underlying insect locomotion. We are also grateful for lengthy discussions on adaptation with Dr. Goran Djordjevic at the Johns Hopkins' Laboratory for Human Motor Learning. Thanks also to Sean Bailey, Edward Froehlich and the other members of the Biomimetics team at CDR. Funding was provided by the Office of Naval Research under grant N00014-98-1-0669.

6. References

- [1] Ahn, A N; Full, R J. 1997. "A motor and a brake: Similar EMGs in two adjacent leg extensor muscles result in completely different function." *American Zoologist*. 37:107A.
- [2] Full, R.J., Autumn, K., Chung, J.I., Ahn, A., "Rapid negotiation of rough terrain by the death-head cockroach." *American Zoologist*. 38:81A. 1998.
- [3] Kubow, T.M., Full, R.J., "The role of the mechanical system in control: A hypothesis of self-stabilization in hexapedal runners." *Phil. Trans. Roy. Soc. London B*. 354, 849-862. 1999.
- [4] Meijer, K., Full, R.J., "Stabilizing properties of invertebrate skeletal muscle." *American Zoologist*. In press.
- [5] Clark, J. E., Cham, J. G., Bailey, S. A., Froehlich, E. M., Nahata, P. K., Full, R. J. and Cutkosky, M. R., *Intl. Conf. Robotics and Automation (ICRA2001)*, Seoul, Korea, May 21-26 2001.
- [6] Bailey, S. A., Cham, J. G., Cutkosky, M. R., and Full, R. J., "Biomimetic Mechanisms via Shape Deposition Manufacturing," in *Robotics Research: the 9th International Symposium*, J. Hollerbach and D. Koditschek (Eds), Springer-Verlag, London, 1999.
- [7] Raibert, M. H., "Legged robots that balance." MIT Press, Cambridge, MA, 1986.
- [8] Koditschek, D. E. and Buhler, M., "Analysis of a Simplified Hopping Robot," *International Journal of Robotics Research*, 10:6, 587-605. 1991.
- [9] Ringrose, R., "Self-stabilizing running," *IEEE ICRA Proceedings*, Albuquerque, NM, 1997.
- [10] Berkemeier, M. D. and Desai, K.V., "A Comparison of Three Approaches for the Control of Hopping Height in Legged Robots." Submitted to the *International Journal of Robotics Research*, 1998.
- [11] Komsuoglu, H. and Koditschek, D. E., "Preliminary Analysis of a Biologically Inspired 1-DOF 'Clock' Stabilized Hopper", *Proceedings of World Multiconference on Systemics, Cybernetics and Informatics (SCI2000)*, Orlando, USA, July 23-26, 2000, Vol IX, pp 670-675.
- [12] Garcia, M., Kuo, A., Peattie, A. M., Wang, P. C. and Full, R. J., "Damping and Size: Insights and Biological Inspiration" in *Proc. of the Intl. Symp. on Adaptive Motion of Animals and Machines*, Montreal, Canada, August 2000.
- [13] Sastry, S. "Nonlinear Systems: Analysis, Stability and Control". Springer Verlag. 1999.
- [14] DeCarlo, R., Branicky, M., Pettersson, S., and Lennartson B., "Perspectives and Results on the Stability and Stabilizability of Hybrid Systems" *Proceedings of the IEEE*, July 2000, pp. 1069-1082.

Appendix

Equations of Motion

The equations of motion for the one-DOF hopper in Figure can be written, in normalized coordinates, as:

$$\dot{X} = AX + B$$

Where A and B are defined as:

$$A = \begin{bmatrix} 0 & 1 \\ -w^2 & -2\zeta w \end{bmatrix} \quad B = \begin{bmatrix} 0 \\ f(t) - 1 \end{bmatrix} \quad \left. \vphantom{\begin{matrix} A \\ B \end{matrix}} \right\} \quad (x \leq 0)$$

during the stance, or ground-contact phase, and:

$$A = \begin{bmatrix} 0 & 1 \\ 0 & 0 \end{bmatrix} \quad B = \begin{bmatrix} 0 \\ -1 \end{bmatrix} \quad \left. \vphantom{\begin{matrix} A \\ B \end{matrix}} \right\} \quad (x > 0)$$

during the airborne, or ballistic, phase. w is the natural frequency and ζ is the damping ratio of the mass-spring-damper system. The thrust force $f(t)$ is determined by the open-loop motor control pattern:

$$f(t) = \begin{cases} 0 & t_{on} < t \leq \tau \\ T_n & 0 < t \leq t_{on} \end{cases}$$

where T_n is the normalized thrust magnitude. Here, t is reset to $t=0$ when t reaches τ . This system is treated as a piecewise affine linear hybrid dynamic system with continuity of state at the mode transitions [14]. The three modes are termed "AIR" (airborne phase), "ON" (stance phase with active thrust) and "OFF" (stance phase with zero thrust). The time solutions of the state vector $X(t)$ for the three modes are:

$$AIR \quad X(t) = \begin{bmatrix} 1 & t \\ 0 & 1 \end{bmatrix} X_0 - \begin{bmatrix} t^2/2 \\ t \end{bmatrix}$$

$$ON \quad X(t) = e^{At} (X_0 - X_{eon}) + X_{eon}$$

$$OFF \quad X(t) = e^{At} (X_0 - X_{eoff}) + X_{eoff}$$

Here, X_o is the state at the beginning of each mode and X_{eon} and X_{eoff} are the equilibrium states for each of the stance modes:

$$X_{eon} = \begin{bmatrix} \frac{T_n - 1}{w^2} \\ 0 \end{bmatrix} \quad X_{eoff} = \begin{bmatrix} -\frac{1}{w^2} \\ 0 \end{bmatrix}$$

Return Maps

In order to study the steady-state motion and local stability of the hopper, we define a return map based on the start time of thrust application, $F(X_n)$ [13]. Since mode switches are both a function of the state and of the open-loop motor pattern, the system trajectory can undergo an indeterminate number of sequences of mode changes. In this analysis, we consider the two hopping behaviors characterized as “Long Thrust” and “Short Thrust.” In “Long Thrust,” we assume that the hopper lands and activates thrust during stance, and that the thrust application duration is long enough to continue until or past lift-off, such that the mode sequence is ON-AIR-OFF. In “Short Thrust,” we assume that the hopper lands and also activates thrust during stance, but that thrust application ends before lift-off, such that the mode sequence is ON-OFF-AIR-OFF.

For “Long Thrust,” we introduce the two timing variables t_{on} (duration of active thrust application) and t_a (1/2 the duration of the airborne phase). To derive the return map, we take advantage of the facts that the take-off velocity (velocity at the ON-AIR mode transition) is the negative of the landing velocity (velocity at the AIR-OFF mode transition) and that this velocity is, in normalized coordinates, equal to t_a . We also take advantage of the fact that the total duration of the modes must equal τ . The return map can then be found by nesting the time solutions for the individual modes in the ON-AIR-OFF sequence:

$$X_{n+1} = F(X_n) = X_{eoff} - e^{A(\tau - 2t_a - t_{on})}(X_{eon} + X_{eoff}) \dots - e^{A(\tau - 2t_a)}(X_n - X_{eon})$$

In order to find the steady-state solutions, or “fixed points,” we impose the constraint $X_n = X_{n+1}$ and seek an expression with only two unknowns:

$$\begin{bmatrix} 0 \\ 0 \end{bmatrix} = \dots$$

$$\begin{bmatrix} 0 \\ t_a \end{bmatrix} - X_{eon} + e^{At_{on}}(X_{eon} - X_{eoff}) + e^{A(\tau - 2t_a)} \begin{bmatrix} 0 \\ t_a \end{bmatrix} + X_{eoff}$$

This set of equations is solved numerically, where our solution vector is $[t_{on} \ t_a]$. If a solution exists, it may be unique or there may be multiple solutions. Once found, t_{on}^* and t_a^* can be used to find X^* , which satisfies:

$$X^* = F(X^*)$$

The return map for the “Short Thrust” mode sequence is similarly found by nesting the time solutions in the ON-OFF-AIR-OFF sequence. Here, we introduce the variables t_{o1} (duration of first OFF stance mode), t_a (1/2 the duration of the airborne phase) and t_{o2} (duration of the second OFF stance mode). The parameter t_{on} is a constant in this case. Again, taking advantage of the fact that the total time duration of the modes must equal τ , the return map is found as:

$$X_{n+1} = F(X_n) = X_{eoff} + (-2e^{At_{o2}}X_{eoff}) \dots - e^{A(\tau - 2t_a - t_{on})}(X_{eon} - X_{eoff}) - e^{A(\tau - 2t_a)}(X_n - X_{eon})$$

Similarly, imposing the steady state constraint, $X_n = X_{n+1}$, we can write the equations as:

$$\begin{bmatrix} 0 \\ 0 \end{bmatrix} = \begin{bmatrix} 0 \\ t_a \end{bmatrix} - X_{eoff} + e^{At_{o1}}(e^{At_{on}} - I)(X_{eon} - X_{eoff}) + \dots - e^{A(\tau - 2t_a)} \begin{bmatrix} 0 \\ t_a \end{bmatrix} + X_{eoff}$$

and solve numerically using a solution vector $[t_{o1} \ t_a]$. As in the previous case, multiple solutions may exist, and it is possible a solution does not exist. Again, if a solution is found, t_{o1}^* and t_a^* can be used to find X^* using the appropriate time solutions.

Local Stability

The local stability of a particular steady-state solution, or fixed point X^* , can be determined by evaluating the Jacobian of the return map at the fixed point, and studying its eigenvalues [13]. The Jacobian, termed M , maps perturbations about the fixed point, δX_n , on one cycle, to perturbations about the fixed point on the next cycle, δX_{n+1} . Therefore, if the eigenvalues of the Jacobian evaluated at X^* are less than unity, the perturbations will decay, which indicates a locally stable steady-state solution:

$$|eig(M(X^*))| < 1$$

where M is defined as:

$$M(X_n) = \frac{\partial}{\partial X_n} F(X_n)$$

In order to obtain this multi-variable derivative, we take advantage of the derivative properties of the matrix exponential:

$$\frac{\partial e^{Af(s)}}{\partial s} = A e^{Af(s)} \frac{\partial f}{\partial s} = e^{Af(s)} A \frac{\partial f}{\partial s}$$

where s is a scalar variable and f a scalar function.

Thus, the Jacobian matrix for the ‘‘Long Thrust’’ case is found to be:

$$M(X^*) = \frac{\partial}{\partial X_n} F(X^*) = 2A(X_{eoff} - X^*) \frac{\partial}{\partial X_n} (t_a) \Big|_{X^*} + \dots$$

$$A e^{At_{off}^*} (X_{eon} + X_{eoff}) \frac{\partial t_{on}}{\partial X_n} \Big|_{X^*} - e^{A(\tau^* - 2t_a^*)}$$

Where the expression has been simplified by using the steady state condition that $X^* = F(X^*)$. In order to find the expressions ct_a/cX_n and ct_{on}/cX_n , we use the take-off condition:

$$\begin{bmatrix} 0 \\ t_a \end{bmatrix} = X_{eon} + e^{At_{on}} (X_n - X_{eon})$$

and decompose each row and take derivatives to find:

$$\frac{\partial t_a}{\partial X_n} \Big|_{X^*} = \begin{bmatrix} 0 & 1 \end{bmatrix} e^{At_{on}^*} \left[A(X^* - X_{eon}) \frac{\partial t_{on}}{\partial X_n} \Big|_{X^*} + I \right]$$

$$\frac{\partial t_{on}}{\partial X_n} \Big|_{X^*} = - \left[\begin{bmatrix} 0 & 1 \end{bmatrix} e^{At_{on}^*} (X^* - X_{eon}) \right]^{-1} \begin{bmatrix} 1 & 0 \end{bmatrix} e^{At_{on}^*}$$

Similarly, the Jacobian matrix for the ‘‘Short Thrust’’ case has been found to be:

$$M(X^*) = \frac{\partial}{\partial X_n} F(X^*) = 2A(X_{eoff} - X^*) \frac{\partial}{\partial X_n} (t_a) \Big|_{X^*} + \dots$$

$$2A e^{At_{o2}^*} (X_{eoff}) \frac{\partial t_{o1}}{\partial X_n} \Big|_{X^*} - e^{A(\tau^* - 2t_a^*)}$$

where $\delta t_a/\delta X_n$ and $\delta t_{on}/\delta X_n$, are found by using the rows of the take-off condition:

$$\begin{bmatrix} 0 \\ t_a \end{bmatrix} = X_{eoff} + e^{At_{o1}} (X_{eon} - X_{eoff}) + e^{At_{on}} (X_n - X_{eon})$$

and taking the derivatives:

$$\frac{\partial t_a}{\partial X_n} \Big|_{X^*} = \begin{bmatrix} 0 & 1 \end{bmatrix} e^{At_{o1}^*} \dots$$

$$\left[A(X_{eon} - X_{eoff}) + e^{At_{on}^*} (X^* - X_{eon}) \right] \frac{\partial t_{o1}}{\partial X_n} \Big|_{X^*} + e^{At_{on}^*}$$

$$\frac{\partial t_{o1}}{\partial X_n} \Big|_{X^*} = \dots$$

$$\left[\begin{bmatrix} 0 & 1 \end{bmatrix} e^{At_{o1}^*} (X_{eoff} - X_{eon}) - e^{At_{on}^*} (X^* - X_{eon}) \right]^{-1} \dots$$

$$\begin{bmatrix} 1 & 0 \end{bmatrix} e^{A(t_{on}^* + t_{o1}^*)}$$